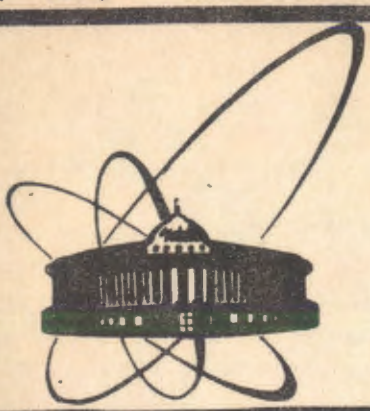

сообщения
объединенного
института
ядерных
исследований
дубна

E13-91-427

Yu.A.Batusov, L.M.Soroko, V.V.Tereshchenko

FOURIER TRANSFORM MICROSCOPE OF THE DIRECT OBSERVATION FOR NUCLEAR EMULSION

1991

1. INTRODUCTION

The information about the tracks of the charged particles in the nuclear emulsion is of the three-dimension (3D) character and application of the picture processing algorithms developed for the plane objects[1,2] to 3D-objects was considered as questionable during a long time. Only in 1981 a new technique of nuclear emulsion viewing and processing was proposed[3] to increase the productivity of the searching for particle tracks. To this end a nuclear emulsion layer is illuminated by the convergent beam of light with its focus in the plane where the FT-pattern of the 3D-object is produced. This far field diffraction picture can be observed directly or viewed through a suitable imaging system. With this technique the scanning operation in depth proved to be completely unnecessary. Besides, the X-Y scanning can be executed with nuclear emulsion in motion. Due to these features this approach opens new scopes of the automation of the searching for particle tracks.

No information about the position of the particle track is lost in the mesooptical Fourier transform microscope (MFTM) which contains the meso-optical element with ring response[4-7]. Quite recently the MFTM with one-channel photodetectors has been tested experimentally[8,9]. Meanwhile the features of the very early FT microscope[3] are left unknown in full scope.

In this paper the FT microscope of the direct observation of the tracks of the charged particles in nuclear emulsion is described. The term "direct observation" means that no imaging elements are present in this nontraditional microscope and no images are viewed by the operator or by the photocamera. The only object of the registration and the only source of the information about the particle tracks in the nuclear emulsion is the picture of the 2D-FT of the straight line particle track. The signals from the array of m photodetectors disposed just behind the narrow transmitting slit undergo the radically new digital processing in accordance with the working flow chart given in this paper. The general theory of this new device is presented. The net effect of the proposed processing algorithms is discussed. The noise immunity of this device is demonstrated. The results of the experiments with robust registration of the particle tracks with low ionization level are presented. It is shown that with such a system we can detect the particle tracks with linear density of 40 silver grains per 100 μm and with initial signal-to-noise ratio1:3. The recommendations for the searching for the particle tracks of low ionization level in the nuclear emulsion by means of the FT microscope of the direct observation are described.

2. FOURIER TRANSFORM MICROSCOPE OF THE DIRECT OBSERVATION

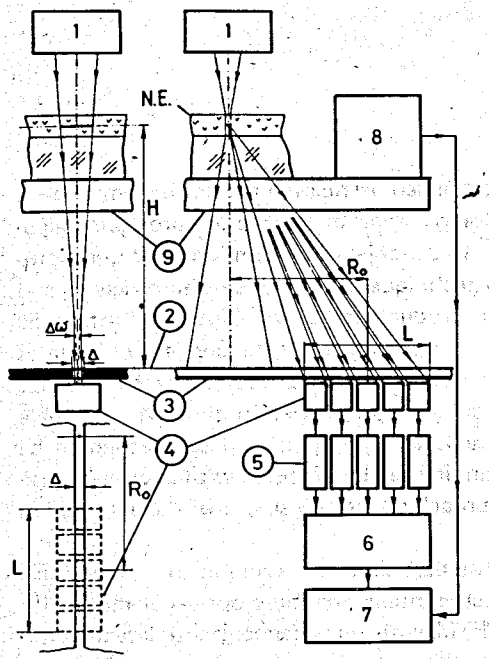

Fig.1. Schematic diagram of the Fourier transform (FT) microscope of the direct observation: 1 — source of the convergent light beam, 2 — FT-plane, 3 — transmitting slit, 4 — array of 5 photodetectors, 5 — array of the amplifiers, 6 — interface, 7 — computer, 8 — X-Y-stage, 9 — rotating fork.

The schematic diagram of the Fourier transform (FT) microscope of the direct observation is shown in fig.1. The developed nuclear emulsion layer N.E. is illuminated by the convergent light beam from the source 1. The FT of the straght line particle track in the horizontal plane perpendicular to the optical axis of the microscope is produced in the FT plane 2. The transmitting slit 3 and the array of m photodetectors 4 just behind the narrow transmitting slit 3 are the only elements of the detected unit of this microscope. The signals form photodetectors 4 are amplified by the array of m amplifiers 5, digitized in the interface 6 and then stored in the computer 7. The X-Y stage 8 with a rotating fork 9 are two mechanical elements of this microscope. The digitized signals from m photodetectors 4 undergo various algorithms described below. We see that no imaging elements are indeed present in the FT microscope of the direct observation.

The working flow chart of the device which define some new possibility of our system is shown in fig. 2. The purpose of this chart is to search for the particle tracks with given orientation angle Θ_{XY} and with very small dip angle $\Theta_Z \approx 0$. The X-Y stage 8 is moving stepwise in the direction chosen perpendicular to the expected orientation of the particle track to be searched for.

Under the initiating signal START the X-Y stage 6 moves through one moving step equal to 10 μm. The digitized photosignals from m photodetectors 4 undergo two processing algorithms:

a) multiplication of all m photosignals, Pr(x);
b) exstraction of the m-th root Pr(x), $\sqrt[m]{\ }$ Pr(x);
c) averaging of photosignals, M(x).

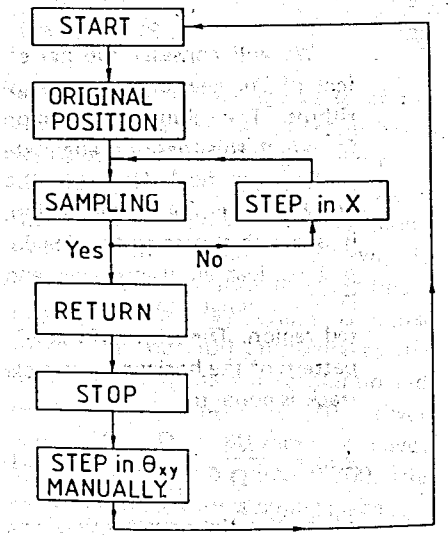

Fig.2. Working flow chart of the device.

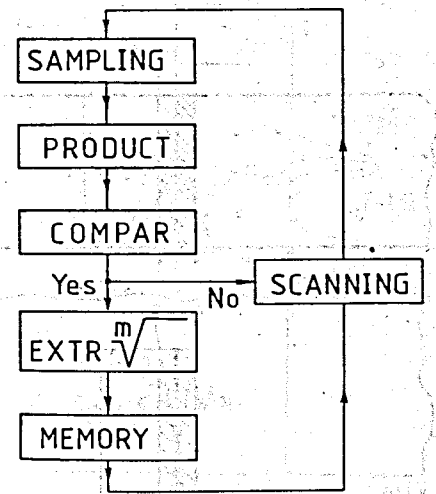

Fig.3. The proposed processing algorithm of the output signals from photodetectors

The m photosignals, $I_i(x)$, i = 1,2,..,m, product signal Pr(x) and the averaging signal M(x) are stored in the computer 7.

If no end signals are issued the X-Y stage 6 performs one more step in X direction and the whole procedure is repeated. If an end signel is present the X-Y stage 6 moves backward into the start position. Between two adjacent scanning operations the operator changes mannually the angular position of the rotating fork 9 with angular increment $\Delta\Theta_{XY}$.

The proposed processing operations accomplished in the computer 7 are shown in fig.3. All sampled signals $I_i(x)$, i = 1,2,..,m, from m photodetectors are multiplied for each x. The product Pr(x) is compared in amplitude with the given comparison level P_0. If the product Pr(x) for some point x is smaller than the comparison level P_0 the output signal will be equal to P_0. If the product Pr(x) exceeds the comparison level P_0, its real value Pr(x) is stored unchanged in the computer memory. These operations are repeated for all positions of the X-Y stage at Y_0 and without scanning along Z-coordinate.

The output signals I(x) , Pr(x) and M(x) represent the array of the 1D-scans in the frame x, Θ_{XY}. The typical number of X-scans is about 200 and the number of the different discret Θ_{XY} orientations is about 20. At the last stage the 2D-plot with axis x Θ_{XY} is calculated and displayed on the computer console.

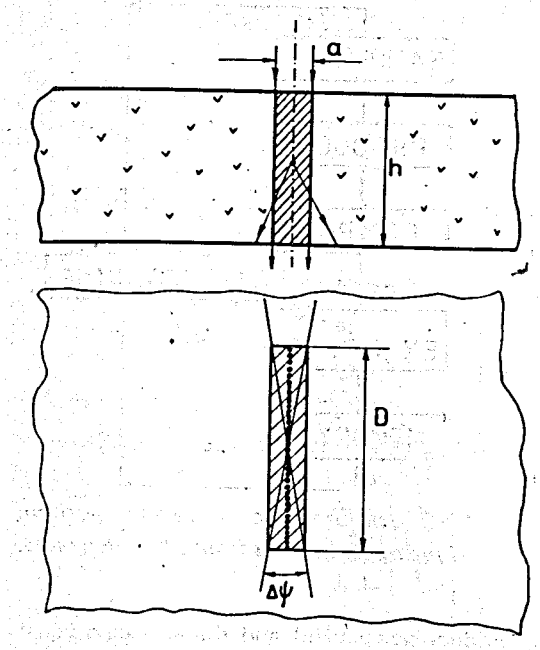

Fig.4. Illuminated region of the FT-microscope of the direct observation: h — thickness of the nuclear emulsion, a — width of the illuminated region, D — length of the illuminated region, Δψ — angular selectivity of the illuminated region.

We will consider the net effect of our new processing algorithms. The illuminated region for which this theory is adequate is shown in fig.4. Here a is the width of the illuminated region, h is the thickness of the developed nuclear emulsion layer and D is the length of the illuminated region. The width of the FT-pattern of the horizontal particle track is equal to

$$\Delta\omega = \frac{\lambda H}{D}, \qquad (1)$$

where λ is the wavelength of the lignt and H is the distance from the nuclear emulsion N.E. to the FT plane 2 in fig.1. The diffraction picture is extending from the diffraction angle $\Theta_d = 0$ to the diffraction angle $\Theta_d^{max} \approx \frac{\lambda}{d}$, where d is the effective width of the straight line particle track. The transmitting slit 3 in fig.1 of the width Δ is placed in the region of this diffraction pattern.

The length of the working part of the transmitting slit 3 is equal to L and the average distance to the optical axis of the microscope is equal to R_0.

Let us consider the end results of the proposed processing algorithms for the case when the signal from the particle track, S, at the output of each photodetector is much smaller than the noise signal, N, from silver grains randomly distributed in the nuclear emulsion.

The intensity of the noise signal N in each of m photodetectors is equal to

$$N = N_0 \pm \sigma(N), \qquad (2)$$

where N_0 is the average noise and q (N) its dispersion. The intensity of the signal from the particle track, S, is equal to

$$S = S_0 \pm \sigma(S), \qquad (3)$$

where S_0 is the average value of the signal S and σ(S) its dispersion. Here we suppose that both signal and noise are random functions with gaussian distributions. Under some real conditions of the searching for particle tracks of low ionization level the linear density of the silver grains is equal to $n = 30$ per 100 μm, whereas the noise N from the whole illuminated region is equivalent to 10^5 silver grains. For D = 3 mm we have: $S_0 = 900$, $\sigma(S) = 30$, $\sigma(N) = 300$. The following inequality is taking place:

$$\sigma(S) < \sigma(N) < S_0 < N_0. \qquad (4)$$

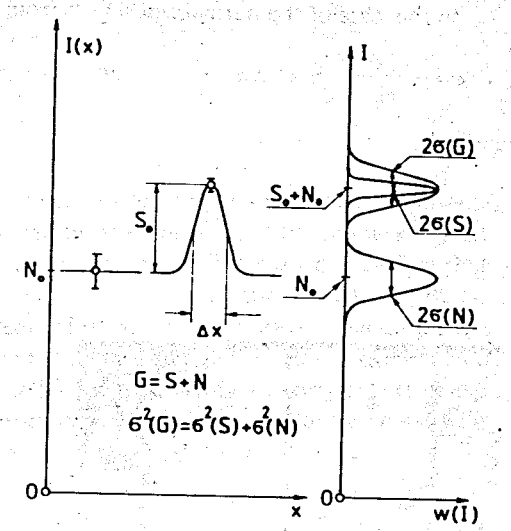

Fig.5. Expected signal from the photodetector for particle track of low ionization level: S — signal, N — noise, G — observed signal, σ(G), σ(N), σ(S) — the corresponding dispersions.

These expected signals are shown in fig.5, where I(x) is the light intensity gathered by some photodetector with X-Y stage in the position (x, y_0). As $\sigma(N) > \sigma(S)$ we assume $\sigma(S) \equiv 0$.

The first experiment which has been performed with our microscope must clear up the statistical nature of the noise N(x). We have found that the dispersion of the product of the noise signals from m photodetectors,

$$\Pi(N) = \prod_{k=1}^{m} \frac{I_k(x)}{N_0^m}, \qquad (5)$$

has the following property:

$$\sigma_n^2(N) = \Sigma\, \sigma_k^2(N) = m\,\sigma^2(N) \qquad (6)$$

with $q_k^2 = \sigma^2(N)$ for all k = 1,2,..., m. This fact shows that the noise N(x) is indeed a noncorrelated random variable. This simplifies the treatment of the problem.

In the case of the processing algorithm with a chain of a transformations:

sampling → multiplication of m-signals → extraction of the m-th root,

we receive the following net result:

$$N_0 \pm \sigma(N) \xrightarrow{\text{multiplication}} N_0 \pm \sqrt{m}\cdot\sigma(N)$$

$$\xrightarrow{\text{extraction of the m-th root}} N_0 \pm \frac{1}{\sqrt{m}}\,\sigma(N). \qquad (7)$$

2. FOURIER TRANSFORM MICROSCOPE OF THE DIRECT OBSERVATION

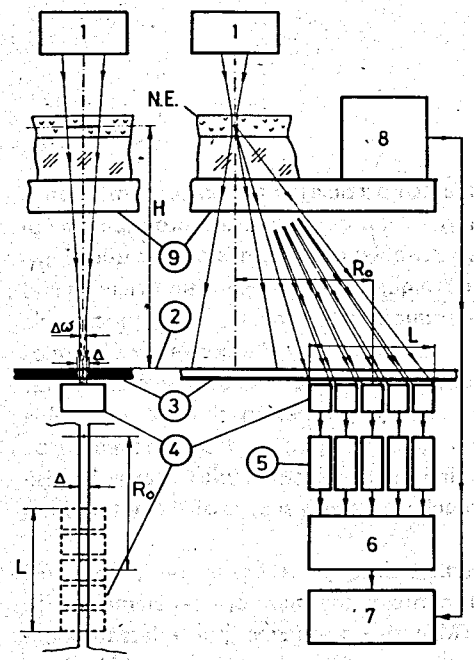

Fig.1. Schematic diagram of the Fourier transform (FT) microscope of the direct observation: 1 — source of the convergent light beam, 2 — FT-plane, 3 — transmitting slit, 4 — array of 5 photodetectors, 5 — array of the amplifiers, 6 — interface, 7 — computer, 8 — X-Y-stage, 9 — rotating fork.

The schematic diagram of the Fourier transform (FT) microscope of the direct observation is shown in fig.1. The developed nuclear emulsion layer N.E. is illuminated by the convergent light beam from the source 1. The FT of the straght line particle track in the horizontal plane perpendicular to the optical axis of the microscope is produced in the FT plane 2. The transmitting slit 3 and the array of m photodetectors 4 just behind the narrow transmitting slit 3 are the only elements of the detected unit of this microscope. The signals form photodetectors 4 are amplified by the array of m amplifiers 5, digitized in the interface 6 and then stored in the computer 7. The X-Y stage 8 with a rotating fork 9 are two mechanical elements of this microscope. The digitized signals from m photodetectors 4 undergo various algorithms described below. We see that no imaging elements are indeed present in the FT microscope of the direct observation.

The working flow chart of the device which define some new possibility of our system is shown in fig. 2. The purpose of this chart is to search for the particle tracks with given orientation angle Θ_{XY} and with very small dip angle $\Theta_Z \approx 0$. The X-Y stage 8 is moving stepwise in the direction chosen perpendicular to the expected orientation of the particle track to be searched for.

Under the initiating signal START the X-Y stage 6 moves through one moving step equal to 10 μm. The digitized photosignals from m photodetectors 4 undergo two processing algorithms:

a) multiplication of all m photosignals, Pr(x);
b) exstraction of the m-th root Pr(x), $\sqrt[m]{\ }$ Pr(x);
c) averaging of photosignals, M(x).

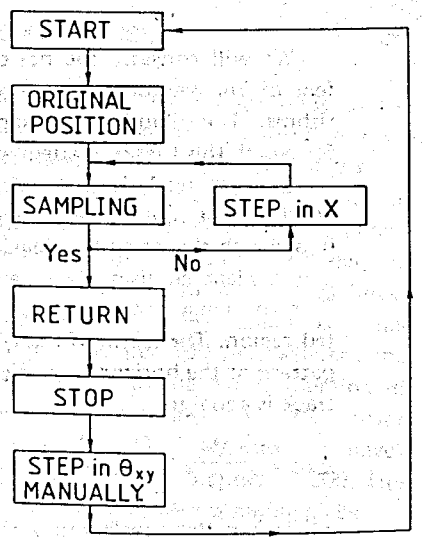

Fig.2. Working flow chart of the device.

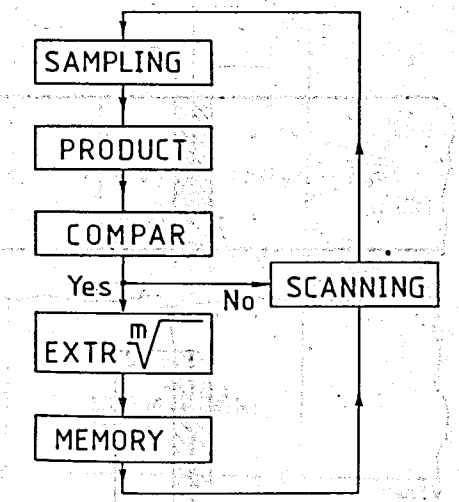

Fig.3. The proposed processing algorithm of the output signals from photodetectors.

The m photosignals, $I_i(x)$, i = 1,2,..,m, product signal Pr(x) and the averaging signal M(x) are stored in the computer 7.

If no end signals are issued the X-Y stage 6 performs one more step in X direction and the whole procedure is repeated. If an end signel is present the X-Y stage 6 moves backward into the start position. Between two adjacent scanning operations the operator changes mannually the angular position of the rotating fork 9 with angular increment $\Delta\Theta_{XY}$.

The proposed processing operations accomplished in the computer 7 are shown in fig.3. All sampled signals $I_i(x)$, i = 1,2,..,m, from m photodetectors are multiplied for each x. The product Pr(x) is compared in amplitude with the given comparison level P_0. If the product Pr(x) for some point x is smaller than the comparison level P_0 the output signal will be equal to P_0. If the product Pr(x) exceeds the comparison level P_0, its real value Pr(x) is stored unchanged in the computer memory. These operations are repeated for all positions of the X-Y stage at Y_0 and without scanning along Z-coordinate.

The output signals I(x) , Pr(x) and M(x) represent the array of the 1D-scans in the frame x, Θ_{XY}. The typical number of X-scans is about 200 and the number of the different discret Θ_{XY} orientations is about 20. At the last stage the 2D-plot with axis x, Θ_{XY} is calculated and displayed on the computer console.

In the case of the normalized signals from m photodetectors with

$$i(x) = \frac{I(x)}{N_0} = (1 \pm \alpha) + s. \qquad (8)$$

and

$$\alpha = \frac{\sigma(N)}{N_0}, \quad s = \frac{S_0}{N_0}, \qquad (9)$$

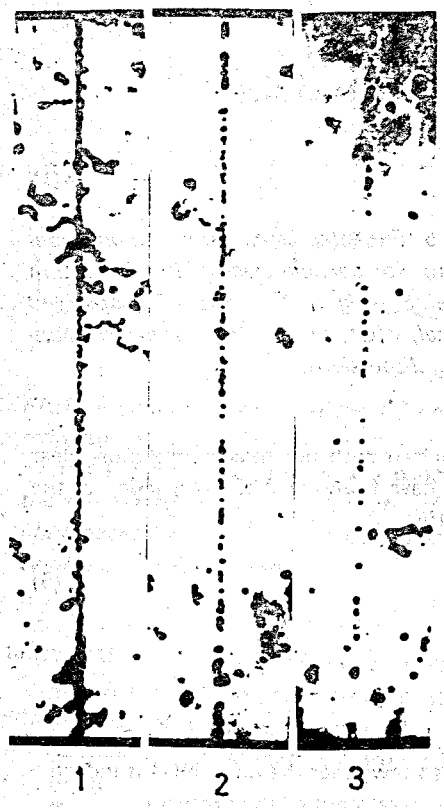

Fig.6. Photographs of the particle tracks used in the experiments: 1) neon neclei, 2) proton with linear density of 100 silver grains per 100 μm, 3) proton with linear density of 40 silver grains per 100 μm.

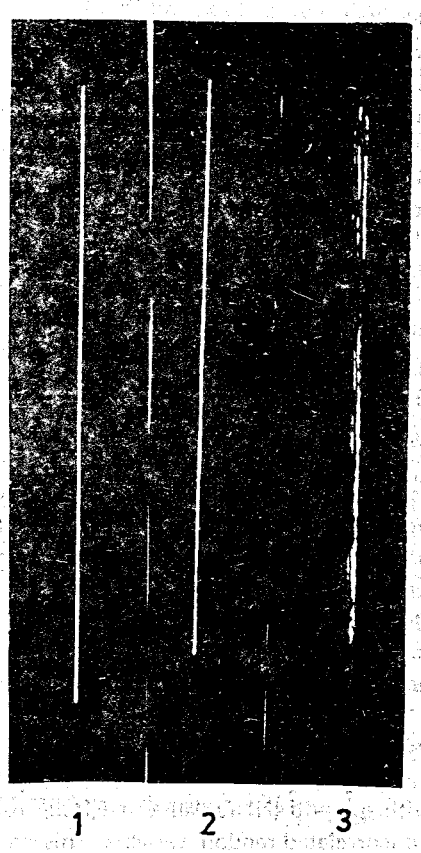

Fig.7. Photographs of the FT-patters of the particle tracks presented in fig.6.

we have

$$(1 \pm \alpha) + s \xrightarrow{\text{multiplication}} (1 \pm \sqrt{m} \cdot \alpha) + ms$$

$$\xrightarrow{\text{extraction of the m-th root}} (1 \pm \frac{\alpha}{\sqrt{m}}) + s. \qquad (10)$$

The noise dispersion is getting $\sqrt{m}$ times smaller under these transformations.

Meanwhile the same result can be attained by the averaging of the primary signals $i_k(x)$, $k = 1,2,...,m$, from m photodetectors. This conclusion follows from the fact that normalized dispersion of the noise $\alpha \ll 1$ and signals-to-noise ratio $s \ll 1$ as well. As these relations are typical ones in the searching for the particle tracks of low ionization level we may offer another, third, algorithm for suppressing of the noise dispersion by a factor of $\sqrt{m}$. For this purpose we must gather noncoherently all components of the diffraciton light which pass through the transmitting slit. This can be done with the help of the light guide comb, which directs all the light into one photodetector.

4. EXPERIMENT

The test expetiments were performed with particle tracks of three types (fig.6): 1) tracks of high ionization level: accelerated neon nuclei of the impulse 4.5 GeV/c per nucleon, 2) tracks of low ionization level: protons with linear density of 100 silver grains per 100 μm, and 3) proton track with linear density of 40 silver grains per 100 μm. The photos of the FT-pattern of these particle tracks in the nuclear emulsion with immersion oil under the cover glass are shown in fig.7.

The signals from eight neon nuclei observed in the MFTM with one channel photodetectors [8] are shown in fig.8. The position of these particle tracks is represented schematically in fig.9 in the frame of the marking grid. To the right from the particle track "8" in fig.8. we see a group of the secondary particles which go parallel to the axis of the beam of primary neon nuclei. These shower particles are shown schematically in fig.19. Their parameters are presented in Table 1, where n is the linear density of silver grains per 100 μm, Z – the depth coordinate of the particle track in the center of the marking grid square, and Θ_Z is the dip angle of the particle track.

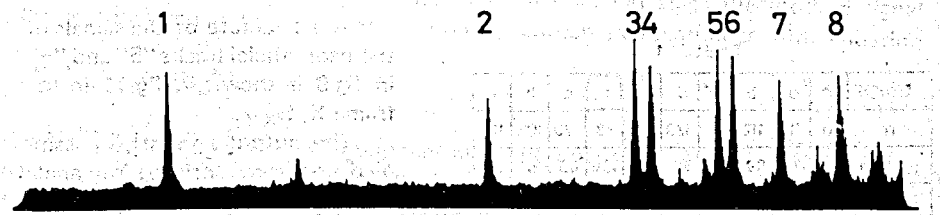

Fig.8. Signals of the neon nuclei observed in the MFTM with one channel photodetectors [8].

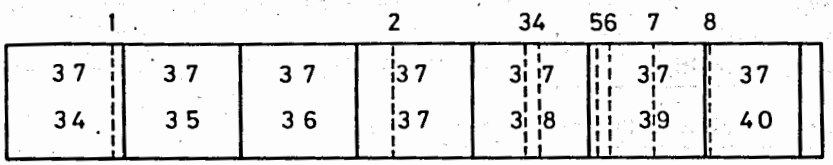

Fig.9. Position of corresponding neon nuclei in the frame of the marking grid.

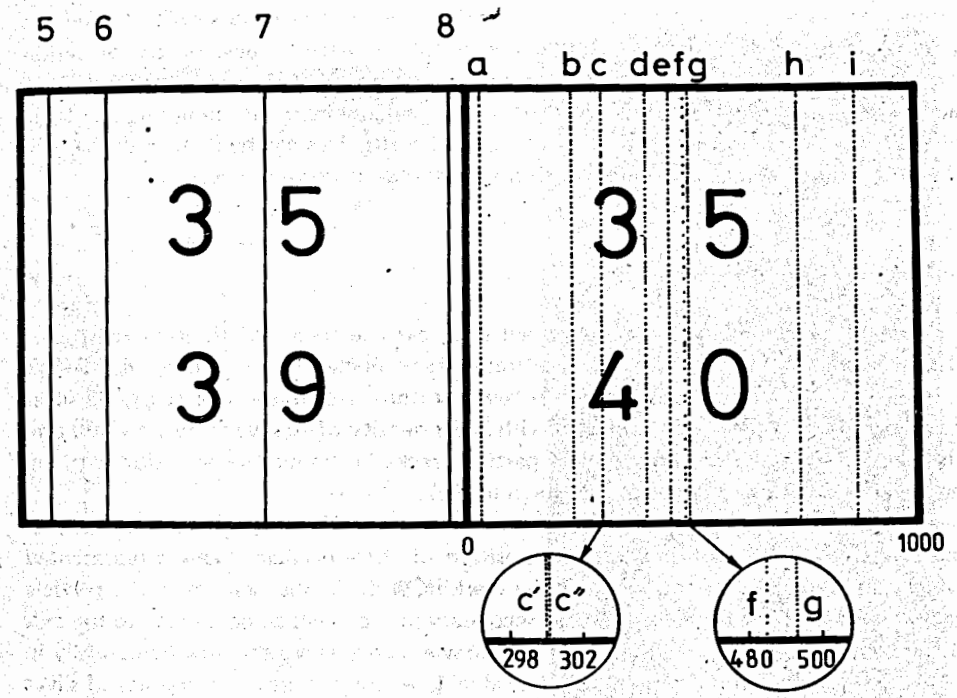

Fig.10. Schematic position of the shower particle tracks in the frame of the marking grid which are to the right from the neon nuclei track "8" in fig.8.

TABLE 1

TRACK	8	a	b	c'c''	d	e	f	g	h	i
n	∞	111	112	111	120	115	38	120	108	112
z, μm	85	75	83	60/126	77	146	106	69	6	30
θ_z °	0	0	.46	.61	2.76	.46	1.22	.23	.61	.46
x, μm	-36	29	244	300	402	450	485	493	740	860

The structure of the signals of the neon nuclei tracks "5" and "6" in fig.9 is shown in fig.11 in the frame X, Θ_{XY}.

The output signals $I_i(x)$ sampled for some orientation angle Θ_{XY} versus transversal coordinate X, i = 1,2,3,4,5 with X-scale in mm are shown in fig.12. The pro-

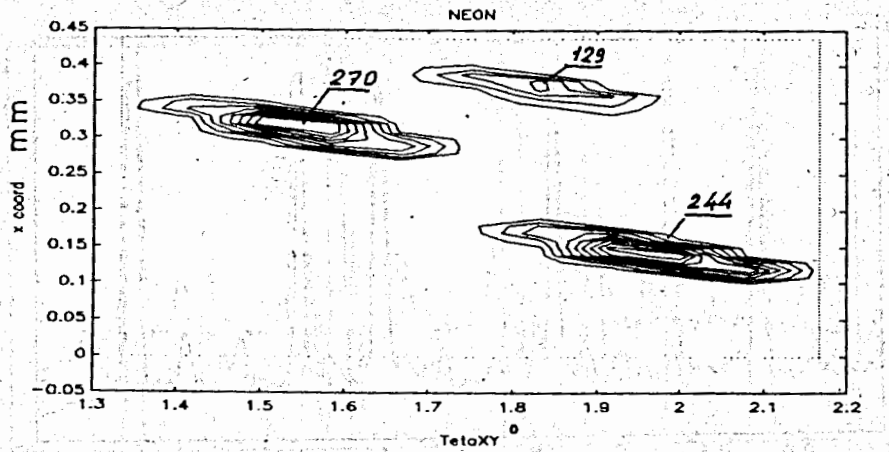

Fig.11. 2D-plot of the two neon nuclei tracks in the frame of X, Θ_{XY} coordinate axes.

duct signals $Pr_{1,2,3}(x)$ and $Pr_{1,2,3,4,5}(x)$ are presented in fig.13. In fig.14 in the same graph we show the 5th root from the product signal $\sqrt[5]{Pr_{1\div5}}(x)$ and the average signal M(x), which are seen to agree with each other in accordance with general theory described in § 3 of this paper.

The most pronounced result of our experiments is the 2D-plot in (X, Θ_{XY}) frame with two peaks of the particle track "f" with linear density of 115 silver grains per 100 μm and of particle track "g" with linear density of 38 silver grains per 100 μm (fig.15). The X-Y stage position was incremented by 5 μm. From fig.15 we may conclude that the particle tracks with linear density of ≈ 40 silver grains per 100 μm can be clearly detected in our microscope with initial signal-to-noise ratio in the average signal M(x) being equal to S/N = 1:3.

In conclusion it should be emphasized that in spite of the fact that two processing algorithms, giving M(x) and $\sqrt[m]{Pr_m}(x)$, are indeed the equivalent ones for weak particle tracks, it is advisable to follow the recommendations which follow by using our FT-microscope of the direct observation for searching for the particle tracks of low ionization level.

At the first stage the digitized output signals from all m photodetectors are multiplied to produce the product signal $Pr_m(x)$. At the second stage the product signal $Pr_m(x)$ is compared with comparator level P_0 chosen in accordance with equation

$$P_0 = N_0^{Pr} + k \cdot \sigma(N_0^{Pr}). \qquad (11)$$

where N_0^{Pr} is the average noise component in the product signal $Pr_m(x)$, $\sigma(N_0^{Pr})$ is the dispersion of the noise signal N_0^{Pr} and k is the number which must be chosen by trials and errors in the range k = 0,5÷5. At the third stage we extract the m-th root from the new signal Pr(x) which has undergone the comparator operation described above.

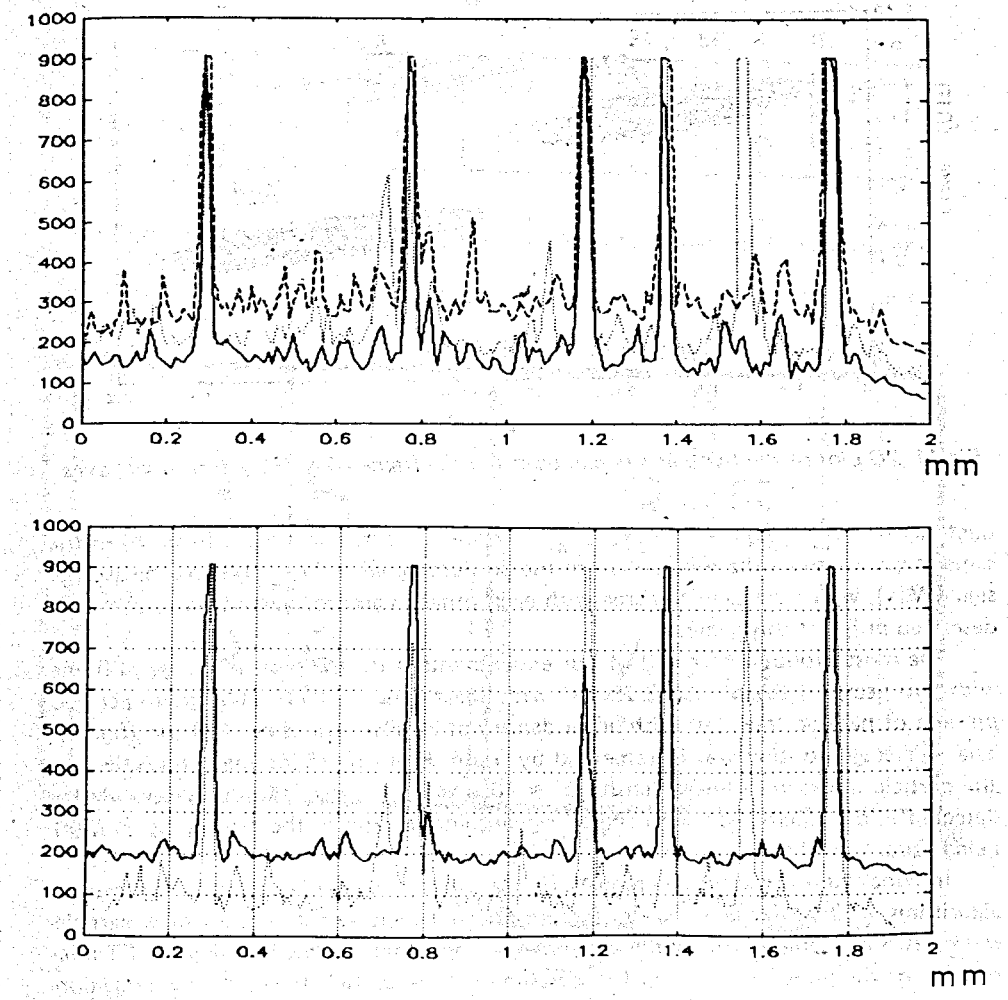

Fig.12. Typical output signals $I_i(x)$, $i = 1,2,3,4,5$ versus x coordinate:
a) ... $I_1(x)$, ——— $I_2(x)$, - - - - $I_3(x)$;
b) ... $I_4(x)$, ——— $I_5(x)$.

From fig.15 we may estimate the angular and the spacial resolution of the device: $\Delta\Theta_{XY} = 12'$ and $\Delta X = 20$ μm. It should be emphasized that axis of the rotating fork in our experiments does not coincide with optical axis of the microscope. Because of this the symmetry axis of the particle track contour in 2D-plots in figs 11 and 15 does not go parallel to the Θ_{XY}-axis.

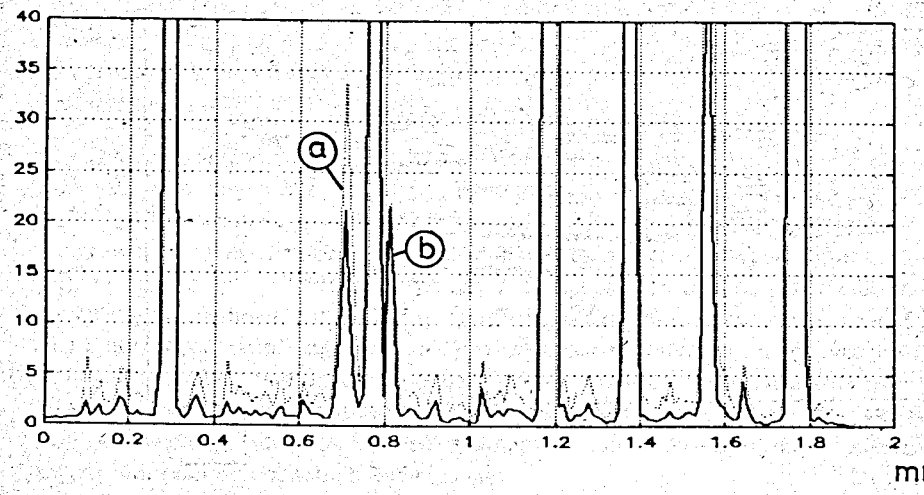

Fig.13. Typical product signals $Pr_{1,2,3}(x)$ (a) and $Pr_{1,2,3,4,5}(x)$ (b).

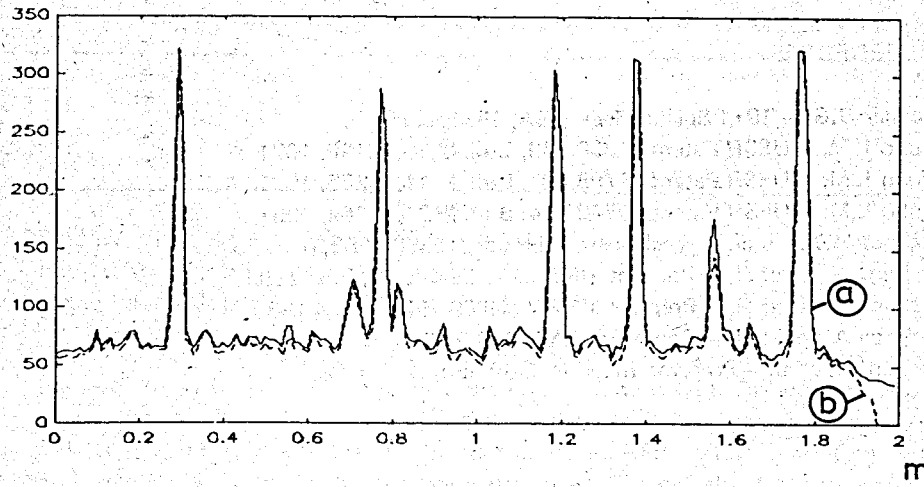

Fig.14. Average signal $M(x)$ (a) and $\sqrt[5]{Pr_5(x)}$ (b) signals for particle tracks of low ionization level, $\Delta = 10$ μm.

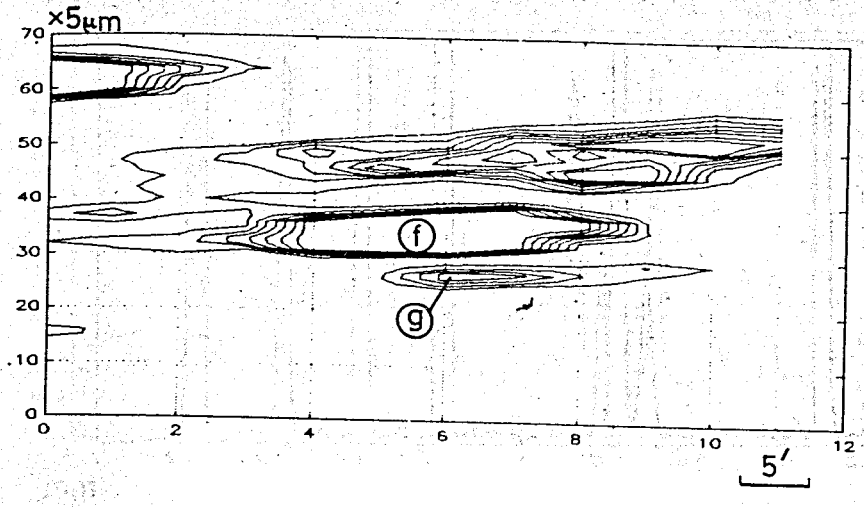

Fig.15. 2D-plot in the frame of X, Θ_{XY} coordinate axis with peaks produced by the proton tracks "f" and "g" (see fig.10).

REFERENCES

1. Falconer D.G. — 1971 Spring Meet. OSA, 1971, p.15.
2. Soroko L.M. — USSR Patent № 300.849, Bull. № 13, p.196, 1971.
3. Soroko L.M. — USSR Patent № 708.807, Bull. № 11, p.265, 1981.
4. Soroko L.M. — USSR Patent № 743.424, Bull. № 21, p.262, 1981.
5. Astakhov A.Ya. et al. — Nucl. Instr. Methods, 1989, A283, p.13-23.
6. Astakhov A.Ya. et al. — Preprint JINR, D13-89-449, Dubna, 1989.
7. Astakhov A.Ya. et al. — Preprint JINR, D13-89-450, Dubna,1989.
8. Astakhov A.Ya. et al. — Commun. JINR P13-91-299, Dubna,1991.
9. Kisvaradi A. et al. — Preprint JINR, D13-89-550, Dubna,1989.

Received by Publishing Department
on September 24, 1991.